RESEARCH

Dipeptidyl peptidase-4 marks distinct subtypes of human adipose stromal/stem cells with different hepatocyte differentiation and immunoregulatory properties

Yu Zhang[1†], Mingxi Hua[2,3†], Xuqing Ma[1], Weihong Li[4], Yuqi Cao[1], Xueya Han[1], Xiaowu Huang[5] and Haiyan Zhang[1,6*]

Abstract

Background Human adipose-derived stromal/stem cells (hASCs) play important roles in regenerative medicine and numerous inflammatory diseases. However, their cellular heterogeneity limits the effectiveness of treatment. Understanding the distinct subtypes of hASCs and their phenotypic implications will enable the selection of appropriate subpopulations for targeted approaches in regenerative medicine or inflammatory diseases.

Methods hASC subtypes expressing dipeptidyl peptidase-4 (DPP4) were identified via fluorescence-activated cell sorting (FACS) analysis. DPP4 expression was knocked down in DPP4$^+$ hASCs via DPP4 siRNA. The capacity for proliferation, hepatocyte differentiation, inflammatory factor secretion and T-cell functionality regulation of hASCs from DPP4$^-$, DPP4$^+$, and control siRNA-treated DPP4$^+$ hASCs and DPP4 siRNA-treated DPP4$^+$ hASCs were assessed.

Results DPP4$^+$ hASCs and control siRNA-treated DPP4$^+$ hASCs presented a lower proliferative capacity but greater hepatocyte differentiation capacity than DPP4$^-$ hASCs and DPP4 siRNA-treated DPP4$^+$ hASCs. Both DPP4$^+$ hASCs and DPP4$^-$ hASCs secreted high levels of vascular endothelial growth factor-A (VEGF-A), monocyte chemoattractant protein-1 (MCP-1), and interleukin 6 (IL-6), whereas the levels of other factors, including matrix metalloproteinase (MMP)-1, eotaxin-3, fractalkine (FKN, CX3CL1), growth-related oncogene-alpha (GRO-alpha, CXCL1), monokine induced by interferon-gamma (MIG), macrophage inflammatory protein (MIP)-1beta, and macrophage colony-stimulating factor (M-CSF), were significantly greater in the supernatants of DPP4$^+$ hASCs than in those of DPP4$^-$ hASCs. Exposure to hASC subtypes and their conditioned media triggered changes in the secreted cytokine profiles of T cells from healthy donors. The percentage of functional T cells that secreted factors such as MIP-1beta and IL-8 increased when these cells were cocultured with DPP4$^+$ hASCs. The percentage of polyfunctional CD8$^+$ T cells that secreted multiple factors, such as IL-17A, tumour necrosis factor alpha (TNF-α) and TNF-β, decreased when these cells were cocultured with supernatants derived from DPP4$^+$ hASCs.

Conclusions DPP4 may regulate proliferation, hepatocyte differentiation, inflammatory cytokine secretion and T-cell functionality of hASCs. These data provide a key foundation for understanding the important role of hASC

---

†Yu Zhang, Mingxi Hua have contributed equally to this work.

*Correspondence:
Haiyan Zhang
culture@ccmu.edu.cn
Full list of author information is available at the end of the article

Zhang *et al. Stem Cell Research & Therapy*   (2024) 15:338

Page 2 of 20

subpopulations in the regulation of T cells, which may be helpful for future immune activation studies and allow them to be customized for clinical application.

Keywords Human adipose stromal/stem cells, Dipeptidyl peptidase 4, Proliferation, Differentiation, Cytokines, Immunoregulation, T cells, CD8$^+$ T cells

Background

Human adipose-derived stromal/stem cells (hASCs) are adult stem cells that exist in the stromal vascular fraction (SVF) of white adipose tissue; these cells have self-renewal and multidirectional differentiation potential and play important roles in development, postnatal growth, and maintenance of adipose tissue homeostasis [1]. Increasing in vitro and in vivo evidence has revealed the immunomodulatory ability of hASCs [2, 3], which makes them potential candidates for therapy in the context of regenerative medicine and for the treatment of numerous inflammatory diseases [4–7].

The majority of hASC products meet a set of minimal criteria for mesenchymal stem/stromal cells (MSCs), as evaluated under classic culture conditions: they must be plastic-adherent; they must express high levels of CD105 (SH2), CD73 (SH3/4) and CD90; they must lack expression of CD45, CD34, CD14, CD11b, CD19 and human leukocyte antigen-D related (HLA-DR) surface molecules; and they must be able to differentiate into osteoblasts, adipocytes and chondroblasts in vitro [5, 6, 8]. However, MSCs often display substantial batch-to-batch variation in phenotype and function, and these differences are based on the donor, tissue source, culture conditions and passage [8–10]. Variations can also be observed within cell populations [11]. Therefore, an improved understanding of the factors underlying cellular heterogeneity and their phenotypic implications will enable appropriate subpopulations to be sourced and expanded for customized and targeted approaches that consider the treatment objectives in the context of regenerative medicine or inflammatory diseases [12].

Dipeptidyl peptidase-4 (DPP4)/CD26 is a widely expressed protease that exists in a membrane-anchored or soluble form and can affect cell proliferation, differentiation, and immune activity [13–16]. hASCs marked by DPP4 expression were identified in human white adipose tissue (WAT) via single-cell RNA sequencing technology and a fluorescence activated cell sorting (FACS) gating strategy [15, 17]. The enriched DPP4/CD55 ASC subpopulation in the adipose tissue of healthy mice was both necessary and sufficient to maximally improve wound healing [17]. Dpp4$^+$ mouse interstitial progenitor cells contribute to basal adipogenesis in all fat depots and are recruited to support *de novo*

adipogenic expansion of visceral WAT in the context of high fat diet (HFD)-induced obesity [18].

Our previous study revealed that hASCs have the capacity to differentiate into hepatocyte-like cells (HLCs) via a reproducible three-stage method that mimics liver embryogenesis [19]. hASC-derived HLCs have the structural characteristics, secretion ability and metabolic functions of human hepatocytes [19–21]. Accumulating evidence indicates that hASC-derived HLCs constitute an attractive tool for establishing alternative therapies for liver dysfunction [22–25], modelling liver disease [26], and developing targeted drugs [27]. However, whether DPP4 affects the hepatocyte differentiation properties of hASCs is not clear.

hASCs possess specific immunomodulatory characteristics that may make them useful for immune-based therapies[3]. hASCs influence the functions of most immune effector cells via direct contact with immune cells and the secretion of specific cytokines, such as the immunosuppressive cytokines IL-6 and transforming growth factor-β1 (TGF-β1) [28–30]. hASCs support the survival of quiescent B cells predominantly via contact-dependent mechanisms [31]. The immunosuppressive effect of hASCs on T-cell subsets occurs via a reduction in NF-kappaB activation that is mediated by the PD-L1/PD-1 and Gal-9/TIM-3 pathways [32]. CCL20$^+$CD14$^+$ monocytes and IL-6 activate DPP4$^+$ hASCs to differentiate towards a proadipogenic phenotype, leading to the formation of creeping fat [33]. However, the specific immunomodulatory effects of DPP4$^+$ hASCs on T cells and cytokine secretion are not clear.

In this study, DPP4$^+$ and DPP4$^-$ cell subpopulations were isolated from hASCs in vitro. The differences in proliferation and hepatocyte differentiation capacity, cytokine secretion profiles, and immunomodulatory effects on T cells between the DPP4$^+$ and DPP4$^-$ hASC subpopulations were investigated.

Methods

Cell culture and differentiation

hASCs were generated as described in our previous report [19]. hASCs were maintained in DMEM/F-12 (Invitrogen, Grand Island, NY, USA) supplemented with 10% fotal bovine serum (FBS, Invitrogen), 100 U/mL penicillin, and 100 μg/mL streptomycin. At 80% confluence, the cells were passaged with 0.05% trypsin and

Zhang *et al. Stem Cell Research & Therapy* (2024) 15:338

Page 3 of 20

0.02% EDTA (Sigma Aldrich, St. Louis, MO, USA) and plated at a density of 5000 cells/cm². Cells from passages four to six were used in this study.

Definitive endodermal differentiation was performed as described in our previous report [19]. Briefly, hASCs were plated on dishes (Nunc) coated with collagen I (Invitrogen) and cultured in DMEM/F-12 (Invitrogen) supplemented with 10% FBS, 100 U/ml penicillin and 100 μg/ml streptomycin at 37 °C with 5% CO_2. Once the cells reached 90% confluence, they were washed twice with PBS and incubated with serum-free DMEM/F-12 for 48 h. The cells were then incubated with DMEM/F-12 containing 0.5 mg/ml albumin fraction V (Sigma Aldrich) with 100 ng/mL activin A (Peprotech) for 24 h, 1% insulin-transferrin-selenium (ITS) (Invitrogen) was added to the medium beginning on the second day, and the cells were cultured for 48 h.

For subsequent hepatic differentiation, the medium was changed to MEM/NEAA (Invitrogen), supplemented with 0.5 mg/mL BSA, 1% ITS, 20 ng/mL BMP2 (Peprotech) and 30 ng/mL FGF4 (Peprotech) for 5 days. To allow for hepatocyte maturation, the cells were further treated with 20 ng/mL hepatocyte growth factor (HGF, Peprotech) for 5 days and then 20 ng/mL HGF, 10 ng/mL oncostatin M (OSM, Peprotech) plus 10^{-6} M dexamethasone (DEX, Sigma Aldrich) for another 5 days. The differentiation media were changed every 2 days.

Flow cytometry

For flow cytometric detection of surface antigens, hASCs (1×10^6 cells) were washed and resuspended in staining buffer (FBS) (BD Biosciences, San Jose, CA) containing saturating concentrations (1:100 dilution) of the following conjugated mouse monoclonal antibodies against human antigens (BD Biosciences) on ice for 30 min in the dark: CD90-FITC, CD34-⁻PE, and DPP4-⁻BV421. FITC labelled mouse IgG1κ isotype control, PE labelled mouse IgG2ακ isotype control, BV421 labelled mouse IgG1κ isotype control were also included. The cell suspensions were washed twice and resuspended in FBS for flow cytometry (BD Accuri C6; BD Biosciences) via FLOWJO™ software (TreeStar, Inc., Ashland, OR). The antibodies used are listed in supplementary materials Table S5.

SA-β-galactosidase staining

Senescence β-galactosidase (SA-β-gal) staining was performed with a cellular senescence assay kit (Beyotime Biotechnology, Shanghai, China) following the manufacturer's instructions. Briefly, the cells were treated with SA-β-Gal fixing buffer at room temperature for 15 min. The cells were then washed 3 times with PBS and stained with working solution (10 μl of buffer A, 10 μl of buffer B, 930 μl of buffer C, and 50 μl of X-Gal solution) overnight at 37 °C without CO_2 for 12–16 h. The population of SA-β-Gal- positive cells was determined by counting 15–20 fields in each group, and images were taken using an Axio Imager A2 microscope (Zeiss, Oberkochen, Germany). The percentage of SA-β-gal-positive area was analysed via the plugin Cell Counter in ImageJ software. The SA-β-Gal-positive area was determined as the percentage of cells stained blue particles (light or dark blue) with respect to the total area of the cells.

Immunofluorescence staining

For immunofluorescence analysis, the cells were fixed with 4% paraformaldehyde for 20 min at room temperature, followed by permeabilization with 0.3% Triton X-100 in PBS for 5 min. The cells were rinsed and blocked with 10% goat serum (ZSGB-BIO, Beijing, China) for 60 min at room temperature. The cells were then incubated with the indicated primary antibodies at 4 °C overnight. Following three 5-min washes in PBS with gentle agitation, an Alexa Fluor-conjugated secondary antibody (Invitrogen) at 1:500 was added, and the samples were incubated for 1 h at 37 °C. The antibodies used are listed in supplementary materials Table S5. The nuclei were counterstained with DAPI (Sigma Aldrich). Images of the fluorescently labelled samples were captured via a Leica TCS SP8 STED confocal laser scanning microscope and a Leica TCS SP5 confocal laser scanning microscope (Leica, Wetzlar, Germany). Relative intensities of staining were quantitatively assessed via ImageJ software.

siRNA transfection

hASCs were plated in growth medium 24 h prior to transfection. Small interfering RNA (siRNA) transfection was performed following the manufacturer's protocol as previously described. Briefly, ON-TARGETplus Human DPP4 siRNA (L-004181-00-0005; Dharmacon, Lafayette, LA, USA) or nontargeting siRNAs (D-001810-10-05, Dharmacon) was mixed with transfected DharmaFECT1 (Dharmacon). After a 20-min incubation at room temperature, the complexes were added to the cells at a final siRNA concentration of 50 nM. The medium was replenished with fresh medium for 24 h posttransfection. Experiments were performed 48–72 h after transfection.

Quantitative RT-PCR

The real time reverse transcription polymerase chain reaction (RT-PCR) was performed as previously described [34]. Total cellular RNA was extracted from 3.0×10^5 cells with a RNeasy Mini Kit (QIAGEN, Hilden, Germany) according to the manufacturer's instructions. Reverse transcription of RNA was performed using Superscript III reverse transcriptase and random

Zhang *et al. Stem Cell Research & Therapy*   (2024) 15:338

Page 4 of 20

hexamer primers (Invitrogen). Real-time PCR analysis was performed on a Thermo Fisher Scientific Applied Biosystems QuantStudio 5 system (Applied Biosystems) with SYBR Green PCR Master Mix (Applied Biosystems). The reaction consisted of 10 µl of SYBR Green PCR Master Mix, 1 µl of a 5 µM mixture of forwards and reverse primers, 1 µl of template cDNA, and 8 µl of water in a total volume of 20 µl. Cycling was performed using QuantStudio Design Analysis Software. The relative expression of each gene was normalized against that of 18S rRNA. The primers used are summarized in Table S6.

Cytokine array and secretome analysis
The cells and cell culture supernatants were collected from the DPP4$^+$ hASCs/DPP4$^-$ hASCs group and the control siRNA-treated DPP4$^+$ hASCs/DPP4 siRNA-treated DPP4$^+$ hASCs. The cytokine array experiments were carried out using the Immune Monitoring 65-Plex Human ProcartaPlex™ Panel (Invitrogen) at Laizee Biotech (Beijing, CN). The signals from the ProcartaPlex™ Panel were detected using Luminex 200 (Luminex). Data acquisition and analysis were conducted via Luminex software.

Single-cell multiplex cytokine profiling of peripheral blood mononuclear cells
Peripheral blood samples were collected from healthy volunteers. The blood was diluted 1:1 with phosphate-buffered saline (PBS), and then the peripheral blood mononuclear cells (PBMCs) were separated and enriched with Ficoll-Paque (Amersham Pharmacia Biotech, Sweden) as previously described [35]. The enriched PBMCs were resuspended in fresh complete RPMI-1640 medium (GIBCO, Grand Island, NY, USA) containing 10% FBS at 1×10^6/mL and stimulated with anti-CD3/CD28 (2 µg/mL and 5 µg/mL; Ebioscience) at 37 °C and 5% CO_2 for 4 h [36].

Then, the PBMCs were cocultured at 37 °C, 5% CO_2 for 4 h with cells or supernatant derived from the cells, namely hASCs, DPP4$^+$ hASCs/DPP4$^-$ hASCs, or control siRNA-treated DPP4$^+$ hASCs/DPP4 siRNA-treated DPP4$^+$ hASCs. After stimulation, the cells were stained with phycoerythrin-conjugated anti-human CD4 (BioLegend, San Diego, CA) or Alexa Fluor 647-conjugated anti-human CD8 (BioLegend) at room temperature for 20-min. Enriched T cells were labelled with carboxyfluorescein succinimidyl ester (Thermo Fisher Scientific), rinsed, and resuspended in RPMI medium at a density of 1×10^6/mL with the addition of phorbol 12-myristate 13-acetate (5 ng/mL; MilliporeSigma, Darmstadt, Germany) and ionomycin (500 ng/mL; MilliporeSigma) to be loaded onto a multiplexed antibody-coated IsoCode chip (IsoPlex), which allows for the analysis of thousands of

T cells at the single-cell level for the frequency and intensity of secretion of 32 cytokines. Each IsoCode chip contains approximately 12,000 microchambers prepatterned with a full copy of a 32-plex antibody array according to a previous study [37, 38]. A schematic of the single-cell IsoCode chip used to analyse T-cell functionality and polyfunctionality. The 32-plex antibody array used are summarized in Fig. S5. T cell polyfunctionality means T cells to secrete multiple (> 2) cytokines per cell according to the previous study [38]. Furthermore, the functionality strength index (FSI) of each sample was computed via a prespecified formula, defined as the percentage of functional cells, multiplied by the mean fluorescence intensity (MFI) of the proteins secreted by those cells: FSI_{sample} = (% functional cells in sample) $\sum_{i=1}^{32}$ MFI of secreted protein i of the functional cells. The polyfunctionality strength index (PSI) of each sample was computed according to a previous study [38]: PSI_{sample} = (% polyfunctional cells in sample)$\sum_{i=1}^{32}$ MFI of secreted protein i of the polyfunctional cells.

Statistical analysis
Statistical analysis was performed with GraphPad Prism 9 software. Statistically significant differences were assessed by an unpaired two-tailed Student's t test. Differences were considered significant if $p < 0.05$.

Results
DPP4 is involved in the regulation of hASC proliferation
To determine the DPP4 status of hASCs, we first analysed cell populations defined by the cell surface proteins CD90 and CD34. The results revealed that approximately 98% of the hASCs were positive for CD90 and negative for CD34 (Figs. S1, Fig. 1A), which is consistent with our previous studies [19, 30]. Then, hASCs from three different donors were subjected to FACS analysis of the DPP4$^+$ and DPP4$^-$ cell populations. Relatively substantial donor-dependent variations in the percentage of DPP4$^+$ hASCs from different donors were detected (Fig. S1C). Approximately 33.3% of the cells were CD90$^+$/DPP4$^+$, and 68% were CD90$^+$/DPP4$^-$ from one donor, as presented in Fig. 1B. To further confirm DPP4 expression, the sorted hASCs were analysed via flow cytometry (Fig. 1C). The majority of both DPP4$^+$ hASCs and DPP4$^-$ hASCs exhibited the typical uniform spindle-shaped appearance of morphogenic fibroblasts (Fig. 1D).

To evaluate the proliferation properties of DPP4$^+$ hASCs and DPP4$^-$ hASCs, immunofluorescence analysis was performed. The results revealed that the proportion of Ki67 positive cells among DPP4$^+$ hASCs was significantly lower than that among DPP4$^-$ hASCs (Fig. 2A). To further investigate whether the reduced proliferative capacity of DPP4$^+$ hASCs is responsible for cellular

Zhang *et al. Stem Cell Research & Therapy*   (2024) 15:338

Page 5 of 20

senescence, senescence-associated beta-galactosidase activity (SA-β-gal) staining was performed. The results revealed that the proportion of SA-β-Gal positive DPP4+ hASCs was significantly greater than that of DPP4− hASCs (Fig. 2B). Quantitative RT-PCR indicated that the expression of the galactosidase beta 1 (*GLB1*) gene was upregulated in DPP4+ hASCs (Fig. 2C).

Additionally, the mRNA levels of the cell cycle inhibitor, cyclin-dependent kinase inhibitor 1A (CDKN1A), CDKN2A, and CDKN2B, but not tumour protein p53 (TP53) were significantly greater in DPP4+ hASCs than in DPP4− hASCs (Fig. 2D). The expression levels of SASP-related genes, including insulin like growth factor binding protein 3 (IGFBP3), interleukin 1 receptor type 1 (IL1R1), and interleukin 6 (IL-6), in DPP4+ hASCs were also significantly greater than those in DPP4− hASCs. These data indicated that the proliferative capacity of DPP4+ hASCs was lower than that of DPP4− hASCs.

To investigate the effect of DPP4 on the proliferative capacity of hASCs, DPP4 expression was knocked down in DPP4+ hASCs using DPP4 siRNA (Fig. S2), and the properties of DPP4+ hASCs were evaluated. Immunofluorescence staining revealed that Ki67 expression was significantly greater in DPP4 siRNA-treated cells than in control siRNA-treated cells (Fig. S3A). Moreover, the percentage of positive areas for SA-β-gal staining was also significantly lower in DPP4 siRNA-treated cells than in control siRNA-treated cells (Fig. S3B). The results of quantitative RT-PCR indicated that the mRNA levels of *IGFBP3* but not the *GLB1*, *TGFB1* and *CDKN2B* were also significantly lower in DPP4 siRNA-treated DPP4+ hASCs than in the control siRNA-treated cells (Fig. S3C, D). These data indicated that DPP4 may be directly involved in regulating the proliferation of hASCs.

DPP4+ hASCs have a greater capacity than DPP4− hASCs for differentiation into hepatocytes

Previously, we demonstrated that the activation of Wnt/β-catenin signalling induces definitive endoderm specification, which may mediate hASC differentiation into functional hepatocytes [19, 39]. To compare the ability of DPP4− hASCs and DPP4+ hASCs to differentiate into hepatocyte-like cells (HLCs), hASCs from two groups (DPP4− hASCs and DPP4+ hASCs or control siRNA-treated DPP4+ hASCs and DPP4 siRNA-treated DPP4+ hASCs) were differentiated using a three-stage differentiation protocol, as previously described [19]. The properties of the differentiated cells in the two groups were analysed at the following stages: definitive endodermal progenitor cells (EPCs), hepatic progenitor cells (HPCs) and HLCs during the process of hepatic differentiation of hASCs.

The results of quantitative RT-PCR revealed that the mRNA levels of GATA binding protein 4 (*GATA4*), *GATA6*, sex determining region Y (SRY)-related high-mobility group (HMG) box (SOX) protein 17 *(SOX17)*, and the fork head domain protein *FOXA2*, which is a marker of definitive endoderm cells, were also significantly greater in DPP4+ hEPCs than in DPP4− hEPCs (Fig. S4A). The mRNA levels of definitive endoderm specific transcription factors were lower in DPP4 siRNA-treated DPP4+ hEPCs than in the control siRNA-treated cells (Fig. S4B). Immunofluorescence staining data verified that the relative intensity of FOXA2 staining in DPP4+ hEPCs was greater than that in DPP4− hEPCs (Fig. 3A). Moreover, the protein level of FOXA2 was lower in DPP4 siRNA-treated DPP4+ hEPCs than in control siRNA-treated cells (Fig. 3B). These results indicated that DPP4+ hASCs presented increased EPC differentiation efficiency.

On day 10 of the differentiation process, the expression of α-fetoprotein (AFP), which is a marker of HPCs, in the cells was determined. The results revealed that the protein level of AFP was greater in DPP4+ hHPCs than in DPP4− hHPCs (Fig. 3C). Compared with that in the control siRNA-treated cells, AFP expression was decreased in DPP4 siRNA-treated hHPCs (Fig. 3D).

The expression of albumin (ALB) and glutathione S-transferase alpha2 (GSTA2), which are markers of hepatocytes, was subsequently analysed. The results revealed that the protein levels of ALB and GSTA2 were greater in DPP4+ hHLCs than in DPP4− hHLCs (Fig. 3E, F). The expression of GSTA2 was lower in DPP4 siRNA-treated DPP4+ hHLCs than in control siRNA-treated

(See figure on next page.)
Fig. 1 DPP4− hASCs and DPP4+ hASCs subpopulations were obtained via FACS. **A** Representative images of the immunophenotype of hASCs using flow cytometry after labelling with antibodies against the indicated antigens. hASC subpopulation isolation via FACS using two defined two surface markers (CD90 and CD34). The images on the left indicate the isotype-matched monoclonal antibody control positive-stained cells. The percentage of cells in each quadrant is shown as indicated. **B** Representative images of the immunophenotype of hASCs via flow cytometry after labelling with antibodies against the indicated antigens. hASC subpopulation isolation via FACS using two defined two surface markers (CD90 and DPP4). The images on the left indicate the isotype-matched monoclonal antibody control positive-stained cells. The percentage of cells in each quadrant is shown as indicated. **C** Representative images of the immunophenotype of hASCs via flow cytometry after labelled with antibodies against the indicated antigens. The percentage of cells in each quadrant is shown as indicated. **D** Representative images of hASCs from DPP4− hASCs and DPP4+ hASCs determined via phase-contrast microscopy; scale bars, 200 µm. SSC, side scatter, represents granularity in cell
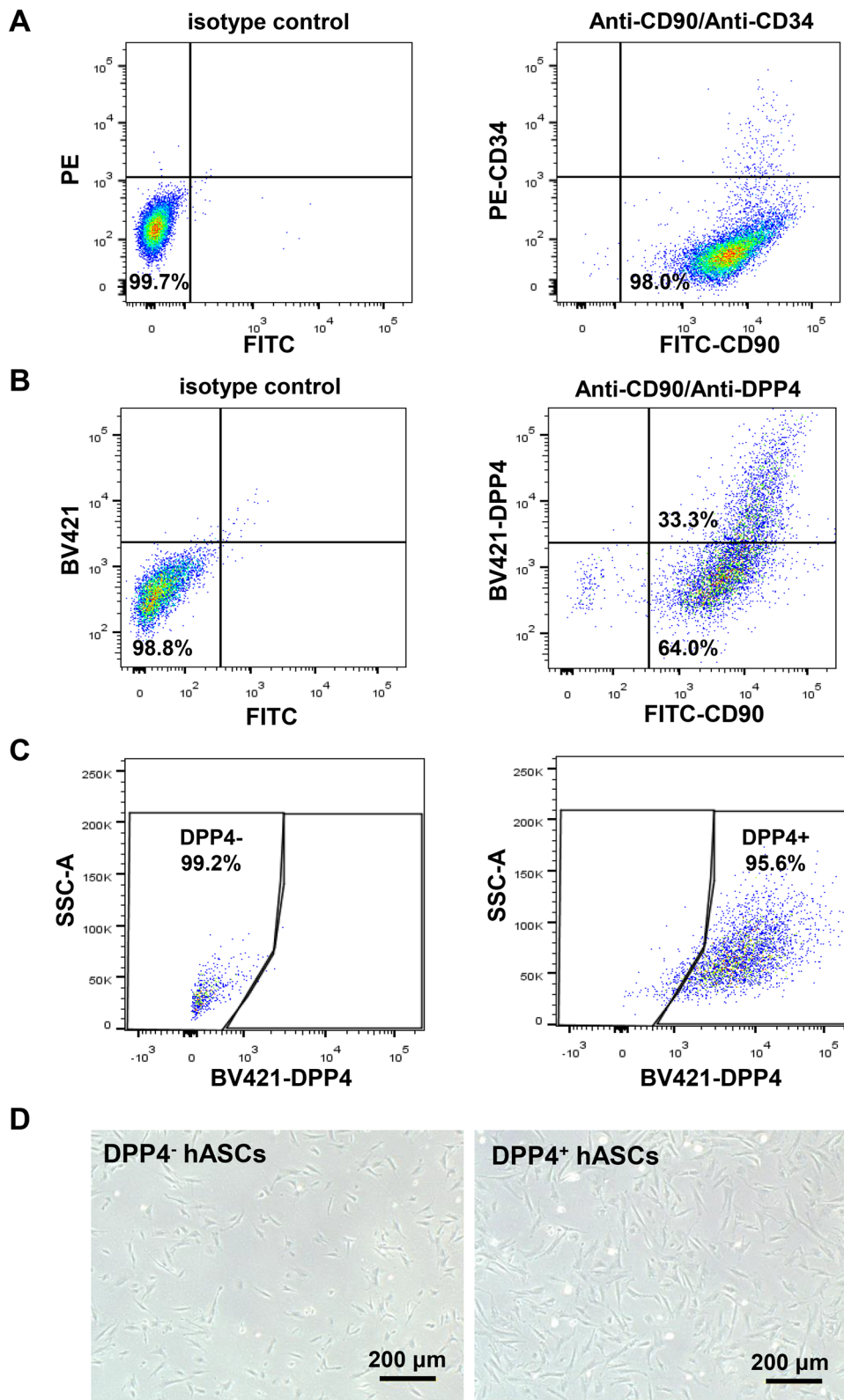
Zhang *et al. Stem Cell Research & Therapy*   (2024) 15:338

Page 6 of 20

Fig. 1 (See legend on previous page.)

Zhang *et al. Stem Cell Research & Therapy*   (2024) 15:338

Page 7 of 20

cells (Fig. S4C). These data indicated that DPP4+ hASCs can be efficiently differentiated into hHLCs by mimicking liver embryogenesis and maturation induction.

DPP4 controls hASC secretion of inflammatory factors

The well-characterized self-renewal properties of hASCs are coupled with their immune modulating function. The immunomodulatory effect of hASCs relies on paracrine effects and the release of various soluble factors [2]. To evaluate the immunomodulatory effects of these cells, 6 growth factors, 33 cytokines, 18 chemokines, and 8 soluble receptors were assessed via the Luminex xMAP approach using the supernatant and cell lysate from hASCs. Radar map profiling revealed different patterns of immunomodulatory factors between the supernatant (Fig. 4A) and the cell lysate (Fig. 4B). The factors with concentrations above 500 pg/mL in the supernatant of hASCs were VEGF-A (3098.025 pg/mL), IL-6 (773.815 pg/mL), MCP-1 (703.915 pg/mL), MIP-3alpha (604.465 pg/mL), and MCP-3 (575.595 pg/mL) (Table S1). The factors presented at concentrations between 100 pg/mL and 500 pg/mL in the supernatant of hASCs included MMP-1, ENA-78, SDF-1alpha, IL-17A, IL-2, IL-27, IL-4, IL-8, LIF, M-CSF, APRIL, IL-2R, TRAIL, and TWEAK (Table S1).

The differentially expressed factors in the supernatant and cell lysate of hASCs were further analysed. The results revealed that the expression of 3 growth factors (MMP-1, VEGF-A, and NGF-beta), 7 chemokines (ENA-78, eotaxin, MCP-1, MCP-2, MCP-3, MIP-3alpha, and SDF-1alpha), 13 cytokines (IFN-alpha, IL-17A, IL-2, IL-20, IL-27, IL-6, IL-7, IL-8, IL-9, LIF, TNF-α, TNF-beta, and TSLP), and 2 soluble receptors (CD30, and CD40L) was significantly upregulated in the supernatants of hASCs compared with the cell lysates of hASCs (Fig. 4C). The factors significantly increased in the cell lysates of hASCs compared with those in the supernatant of hASCs are shown in Fig. 4D. The protein levels of 10 factors did not differ between the supernatant and cell lysates of hASCs (Fig. 4E).

To elucidate whether DPP4 controls hASC secretion of inflammatory factors, the differences in the levels of these factors in the supernatants and cell lysates of DPP4+ hASCs and DPP4− hASCs were further studied. The results revealed that the levels of matrix metalloproteinase (MMP) -1, Eotaxin-3, Fractalkine (FKN, CX3CL1), growth-related oncogene-alpha (GRO-alpha, CXCL1), monokines induced by interferon-gamma (MIG), macrophage inflammatory protein (MIP)-1beta, and macrophage colony-stimulating factor (M-CSF) were significantly greater in the supernatant of DPP4+ hASCs than in that of DPP4− hASCs. The protein level of HGF in the supernatant of DPP4− hASCs was greater than that in the supernatant of DPP4+ hASCs (Fig. 5A, Table S2a).

To investigate the differences in the secretory profiles of hASCs, DPP4− hASCs and DPP4− hASCs, the differentially expressed factors in the supernatant of three groups of hASCs were further analysed. The results revealed that the protein level of Eotaxin-2 and BLC in the supernatant of DPP4− hASCs and DPP4− hASCs was higher than in hASCs. The protein level of HGF, VEGF-A, Eotaxin, Fractalkine, MIG, MIP-3alpha, IL-22, M-CSF, TSLP, and BAFF in the supernatant of DPP4− hASCs and DPP4− hASCs was lower than in hASCs (Table S2b).

The factors with upregulated expression (P <0.05, fold change >1.2) in cell lysates from DPP4+ hASCs and DPP4− hASCs included SCF, VEGF, BLC, ENA-78, eotaxin-3, GRO-alpha, I-TAC, MCP-3, MIG, MIP-1beta, MIP-3alpha, G-CSF, GM-CSF, IFN-alpha, IL-1beta, IL-21, IL-22, IL-6, IL-7, IL-8, IL-9, M-CSF, MIF, APRIL, CD40L, and TRAIL (Fig. 5B and Table S3). The protein level of HGF in both the supernatant and cell lysate of DPP4− hASCs was lower than that in DPP4+ hASCs.

To investigate the effect of DPP4 on inflammatory factor expression in hASCs, the supernatants and cell lysates from control siRNA-treated DPP4+ hASCs and DPP4 siRNA-treated DPP4+ hASCs were studied. The results revealed that the protein levels of 17 factors in the supernatant and 2 factors in the cell lysates of DPP4 siRNA-treated DPP4+ hASCs were significantly greater than

(See figure on next page.)

Fig. 2 Proliferation of DPP4− hASCs and DPP4+ hASCs. **A** Representative image of hASCs in the two groups immunoassayed with an antibody against Ki-67. Histogram showing the difference in the percentage of Ki-67 positive cells between DPP4− hASCs and DPP4+ hASCs. There were 20 fields in each group. Data are presented as mean ± SEM. Scale bars, 50 μm. **B** Representative images of hASCs in the two groups subjected to SA-β-Gal staining. Histogram showing the difference in the percentage of SA-β-Gal positive area between DPP4− hASCs and DPP4+ hASCs. There were 20 fields in each group. n = 3 different experiments. Data are presented as mean ± SEM. Scale bars, 200 μm. Insets: Enlarged image of individual cell was indicated by white arrows. **C** Relative mRNA level of *GLB1* in DPP4− hASCs and DPP4+ hASCs determined by quantitative RT-PCR. The relative expression of the gene was normalized against that of 18S rRNA. Data are presented as mean ± SEM. **D** Relative mRNA levels of *CDKN1A*, *CDKN2A*, *CDKN2B* and *TP53* in DPP4− hASCs and DPP4+ hASCs determined by quantitative RT-PCR. The relative expression of the genes was normalized against that of 18S rRNA. Data are presented as mean ± SEM. **E** Relative mRNA levels of *IGFBP3*, *IL1R1*, *TGFB1* and *IL6* in DPP4− hASCs and DPP4+ hASCs determined by quantitative RT-PCR. The relative expression of the genes was normalized against that of 18S rRNA. Data are presented as mean ± SEM. Significant differences were determined by unpaired two-tailed Student's *t* tests
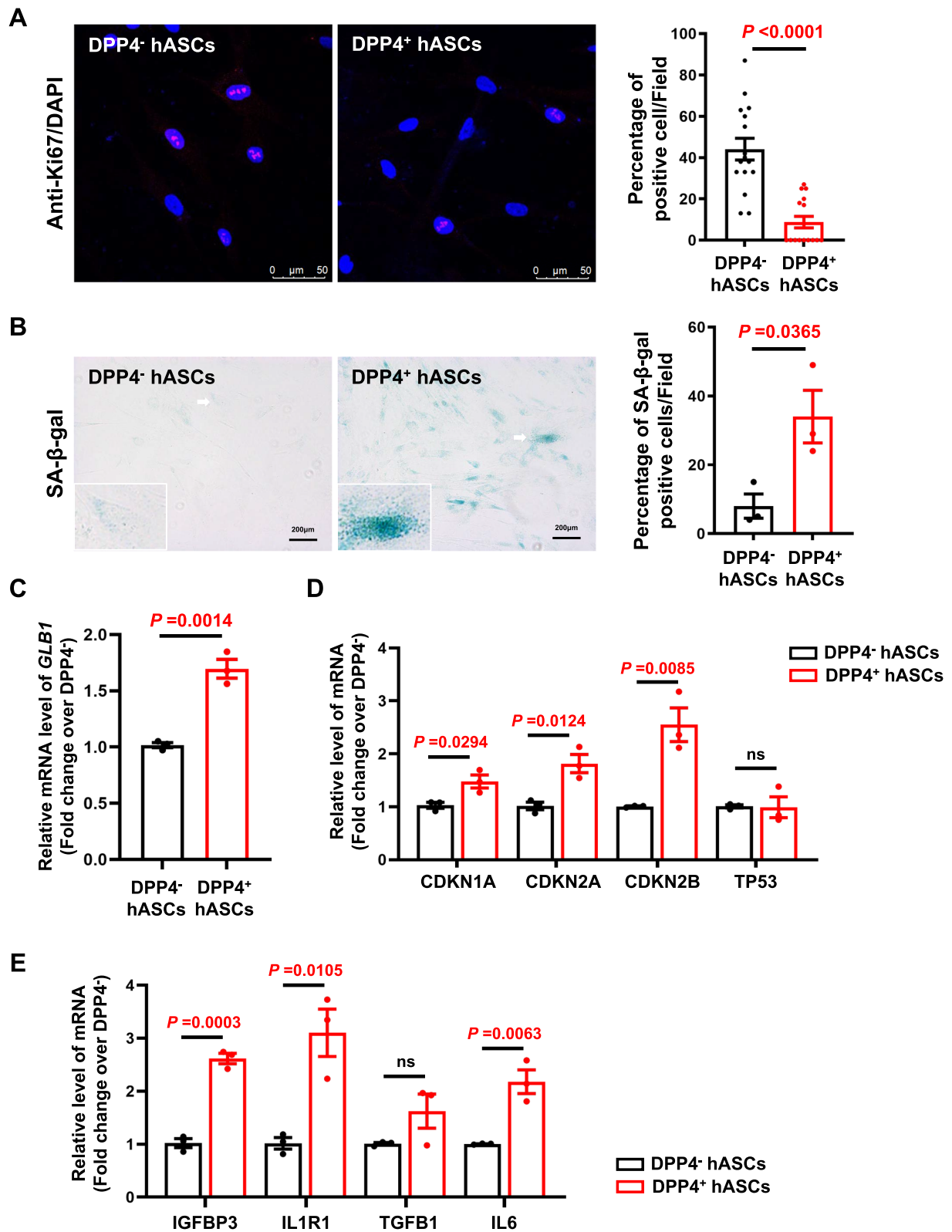
Fig. 2 (See legend on previous page.)

Zhang *et al. Stem Cell Research & Therapy*   (2024) 15:338
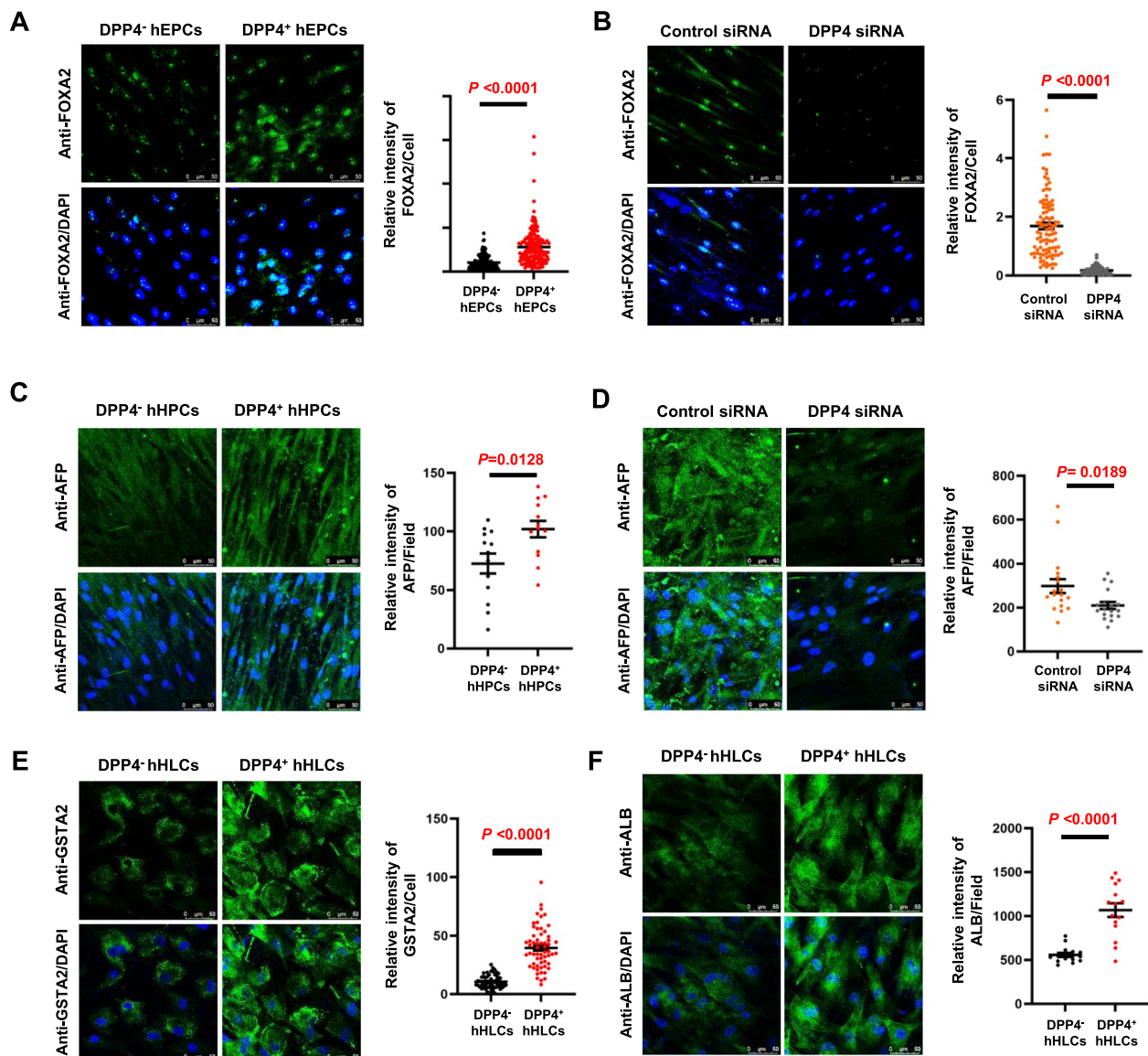
Page 9 of 20

Fig. 3 The differentiation potential of DPP4⁻ hASCs and DPP4⁺ hASCs. **A** Representative images of the expression of FOXA2 in DPP4⁻ hEPCs and DPP4⁺ hEPCs determined by immunofluorescence. Scatter diagram showing the difference in the relative intensity of FOXA2 in cells. There were 60 cells in each group. The data are presented as the means ± SEM. Scale bars, 50 µm. **B** Representative images of the expression of FOXA2 in DPP4 siRNA-treated and control siRNA-treated DPP4⁺ hEPCs determined by immunofluorescence. Scatter diagram showing the difference in the relative intensity of FOXA2 in cells. There were 60 cells in each group. The data are presented as the means ± SEM. Scale bars, 50 µm. **C** Representative images of the expression of AFP in DPP4⁻ hHPCs and DPP4⁺ hHPCs determined by immunofluorescence. Scatter diagram showing the difference in the relative intensity of AFP in the fields. There were 13 fields in each group. The data are presented as the means ± SEM. Scale bars, 50 µm. **D** Representative images of the expression of AFP in DPP4 siRNA-treated and control siRNA-treated DPP4⁺ hHPCs determined by immunofluorescence. Scatter diagram showing the difference in the relative intensity of AFP in fields. There were 18 fields in each group. The data are presented as the means ± SEM. Scale bars, 50 µm. **E** Representative images of the expression of GSTA2 in DPP4⁻ hHLCs and DPP4⁺ hHLCs determined by immunofluorescence. Scatter diagram showing the difference in the relative intensity of GSTA2 in cells. There were 60 cells in each group. The data are presented as the means ± SEM. Scale bars, 50 µm. **F** Representative images of the expression of ALB in DPP4⁻ hHLCs and DPP4⁺ hHLCs determined by immunofluorescence. Scatter diagram showing the difference in the relative intensity of ALB in the fields. There were 15 fields in each group. The data are presented as the means ± SEM. Scale bars, 50 µm. Significant differences were determined by unpaired two-tailed Student's *t* tests

Zhang *et al. Stem Cell Research & Therapy*   (2024) 15:338

Page 10 of 20

those in the supernatant and lysate of control siRNA-treated DPP4+ hASCs (Fig. 5C, Table S4a). Compared with those in control siRNA-treated DPP4+ hASCs, the protein level of HGF in both the supernatant and the cell lysate was greater in DPP4 siRNA-treated DPP4+ hASCs (Fig. 5C, Table S4b).

These data confirmed that hASCs can secrete many important factors that may be involved in distinct immunomodulatory properties, including vascular development and angiogenesis, maintenance of homeostasis, mediation of innate immunity and tissue inflammation. Moreover, the results indicated that DPP4 regulates HGF expression in hASCs.

DPP4 expression in hASCs is involved in the regulation of T-cell polyfunctionality

T-cell immunity plays a critical role in the body's immune defend against infectious diseases, sterile inflammation, tumours, and autoimmune diseases. Once appropriately activated, T cells infiltrate the microenvironment and recognize and defend against antigens. The range of T-cell functions includes the ability to proliferate or induce the proliferation of other cells (through the secretion of growth factors), organize immune responses (by secreting chemoattractants) and carry out effector functions by directly killing infected cells through cytolytic mechanisms or secretion of the cytokines [40].

To determine whether hASCs could regulate the functional properties of T cells, especially their polyfunctionality, which is the ability to secrete multiple (>2) cytokines per cell, a multiplexed antibody-coated chip that allows the analysis of thousands of T cells at the single-cell level to determine the frequency and intensity of secretion of 32 cytokines was used, as described in previous studies [37, 38]. Single-cell functional profiles based on secreted proteins can be categorized into effector (granzyme B, IFN-γ, MIP-1α, perforin, TNF- α, and TNF-β), stimulatory (GM-CSF, IL-2, IL-5, IL-7, IL-8, IL-9, IL-12, IL-15, and IL-21), regulatory (IL-4, IL-10, IL-13, IL-22, TGF-β1, sCD137, and sCD40L), chemoattractive (CCL-11, IP-10, MIP-1β, and RANTES), and inflammatory (IL-1B, IL-6, IL-17A, IL-17F, MCP-1, and MCP-4) groups (IsoCode Chip, Fig. S5). A prespecified T-cell functionality strength index (FSI) and polyfunctionality strength index

(PSI) were combined with cytokine secretion profiles to evaluate T cell functions in activated PBMCs with anti-CD3/CD28 antibodies from health donors cultured with the supernatant of hASCs or hASCs (Fig. S6). The exposure of hASCs to activated PBMCs from healthy donors significantly increased T-cell functionality, including FSI and PSI values (Fig. S7). Therefore, activated PBMCs were used in subsequent studies.

The immunomodulatory effect of hASCs relies on paracrine effects and the release of various soluble factors [2]. To evaluate the effect of hASCs on T-cell functionality, activated PBMCs were cultured with hASCs or the medium of hASCs in vitro for 4 h, after which the FSI, PSI and cytokines secreted by CD4+ T cells or CD8+ T cells were determined. The results revealed that the functional profiles of CD4+ T cells and CD8+ T cells changed when the cells were cultured with hASCs. CD4+ T-cell functions, including effector, stimulatory, chemoattractive, and inflammatory functions, were increased, and the regulatory FSI value was decreased when the cells were cultured with hASCs. CD8+ T-cell functions, including stimulatory and chemoattractive functions, were increased, and the effector FSI and inflammatory FSI values were decreased when the cells were cultured with hASCs (Fig. 6A). Further analysis of the polyfunctionality of T cells revealed increased PSI values in CD4+ T cells, including effector and stimulatory T cells, and decreased PSI values in CD8+ T cells, including effector and inflammatory T cells (Fig. 6B). These results indicate that there is a significant difference in the immunomodulatory effect of hASCs on CD4+ T cells and CD8+ T cells. The reduced PSI in CD8+ T cells cultured with hASCs indicates that hASCs might suppress CD8+ T cell activation or cytokine secretion.

The major cytokines and chemokines induced in CD4+ T cells and CD8+ T cells upon treatment with hASCs were IL-8 and MIP-1beta (Fig. 6C, D). The number of TNF-α-producing functional or polyfunctional CD4+ T cells increased upon treatment with hASCs, whereas the number of CD8+ T cells that produced TNF-α decreased upon treatment with hASCs (Fig. 6C, D). The levels of Granzyme B, RANTES, IL-9, and MPC-4 produced by functional or polyfunctional CD4+ T cells and CD8+ T cells decreased upon treatment with hASCs (Fig. 6C, D).

(See figure on next page.)
Fig. 4 Cytokine secretion and expression in hASCs. **A** Radial bar chart of the protein content in the supernatant of hASCs, as determined via an immune monitoring panel. The number of proteins was 65. **B** Radial bar chart of the protein content in the cell lysates of hASCs, as determined by an immune monitoring panel. The number of proteins was 65. **C-E** Stacked bar charts showing the protein contents in the supernatant and cell lysates from hASCs. **C** The protein contents of factors were significantly greater in the supernatant of hASCs than in the cell lysates of hASCs. **D** The protein contents of factors were significantly greater in the cell lysates of hASCs than in the supernatant of hASCs. **E** The protein contents of factors that were not different between the supernatant and cell lysate of hASCs
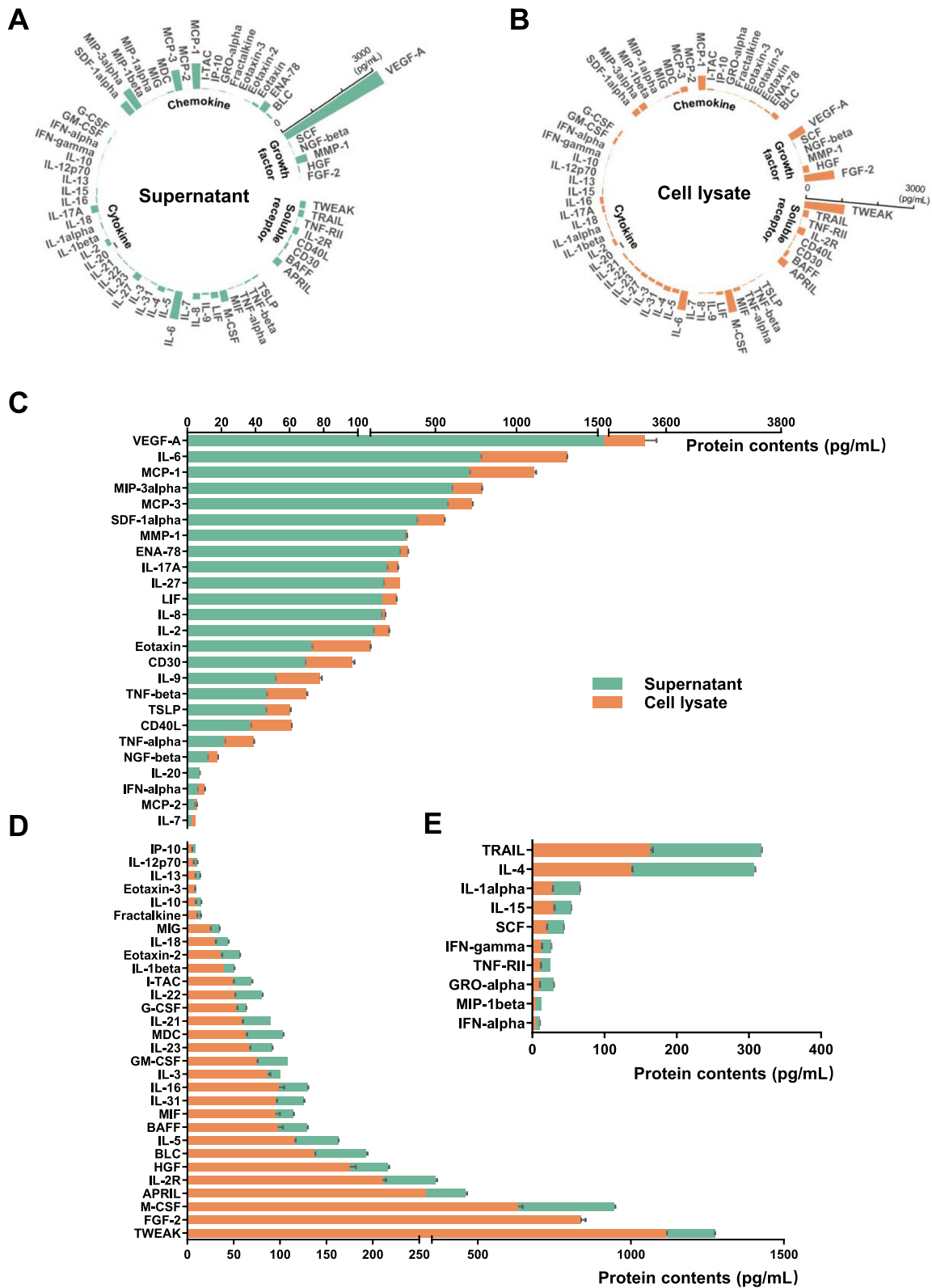
Zhang *et al. Stem Cell Research & Therapy*   (2024) 15:338

Page 11 of 20
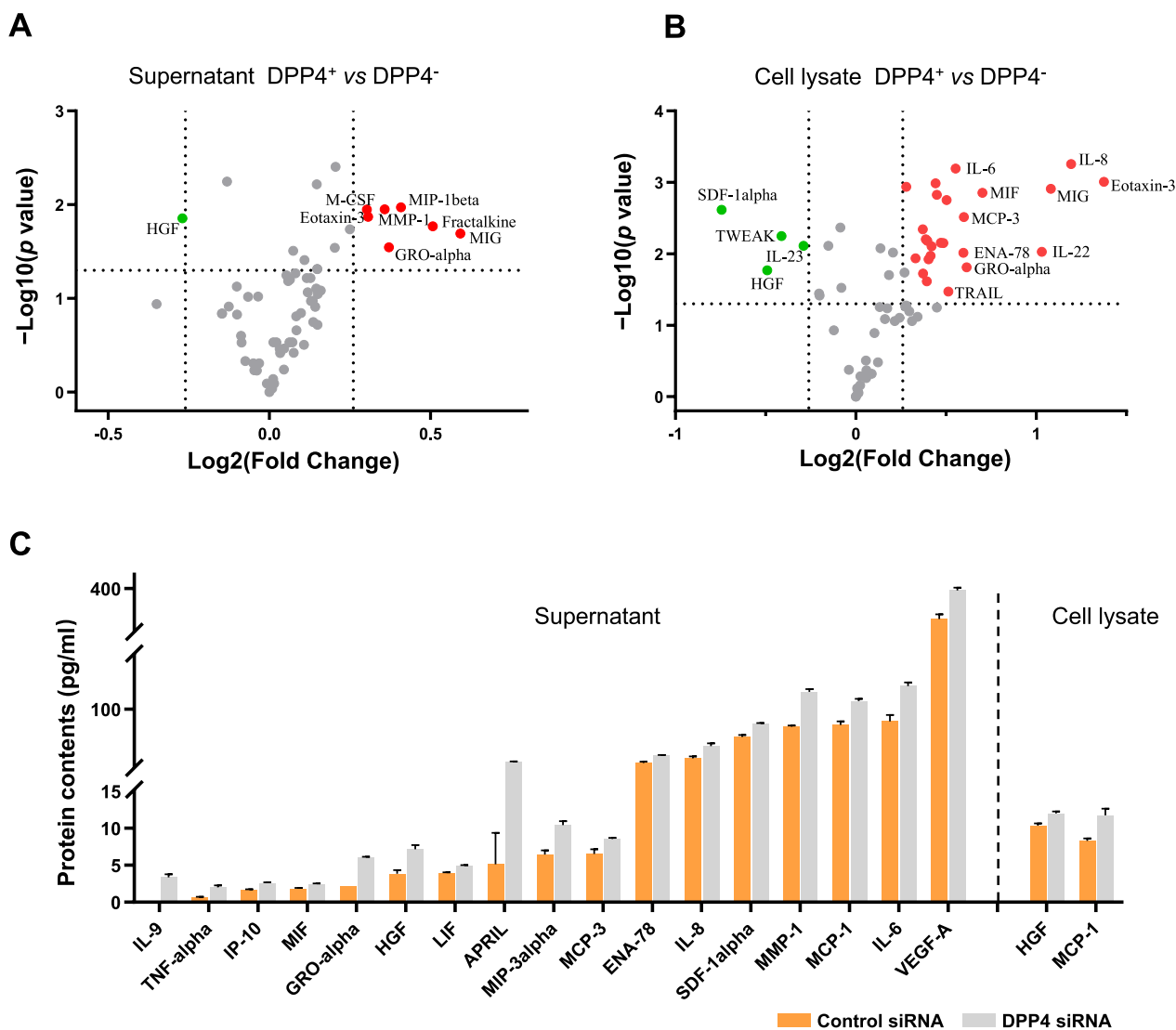

Fig. 4 (See legend on previous page.)

Fig. 5 Regulatory effects of DPP4 on cytokine secretion and expression in hASCs. **A** Scatter matrix showing the fold change and *P* value of protein contents in supernatants from DPP4− hASCs and DPP4+ hASCs. The green dots represent the protein contents of factors that were significantly greater in the supernatant of DPP4− hASCs than in the supernatant of DPP4+ hASCs. The red dots represent the protein contents of factors that were significantly greater in the supernatant of DPP4+ hASCs than in the supernatant of DPP4− hASCs. **B** Scatter matrix showing the fold change and *P* value of protein contents in cell lysates from DPP4− hASCs and DPP4+ hASCs. The green dots represent the protein contents of factors that were significantly greater in the cell lysates of DPP4− hASCs than in the cell lysate of DPP4+ hASCs. Red dots represent the protein contents of factor significantly greater in the cell lysates of DPP4+ hASCs than in the cell lysate of DPP4− hASCs. **C** Histogram showing the protein contents in the supernatant and cell lysates from DPP4+ hASCs treated with control siRNA or DPP4 siRNA

(See figure on next page.)

Fig. 6 Regulation of the polyfunctionality of T cells by hASCs. **A** Stacked bar charts showing the single-cell functionality of PBMCs and PBMCs cocultured with hASCs. **B** Stacked bar charts showing the single-cell polyfunctionality of PBMCs and PBMCs cocultured with hASCs. Polyfunctionality: co-secretion of more than 2 cytokines per cell; each colour corresponds to a specific cytokine or combination of cytokines. **C** Histogram showing the polyfunctional group of CD4+ T cells and CD4+ T cells cocultured with hASCs. **D** Histogram showing the polyfunctional group of CD8+ T cells and CD8+ T cells cocultured with hASCs. **E** Stacked bar charts showing the single-cell functionality of PBMCs and PBMCs treated with the supernatant of hASCs. **F** Stacked bar charts showing the single-cell functionality of PBMCs and PBMCs treated with the supernatant of hASCs. **G** Histogram showing the polyfunctional group of CD4+ T cells and CD4+ T cells treated with the supernatant of hASCs. **H** Histogram showing the polyfunctional group of CD8+ T cells and CD8+ T cells treated with the supernatant of hASCs
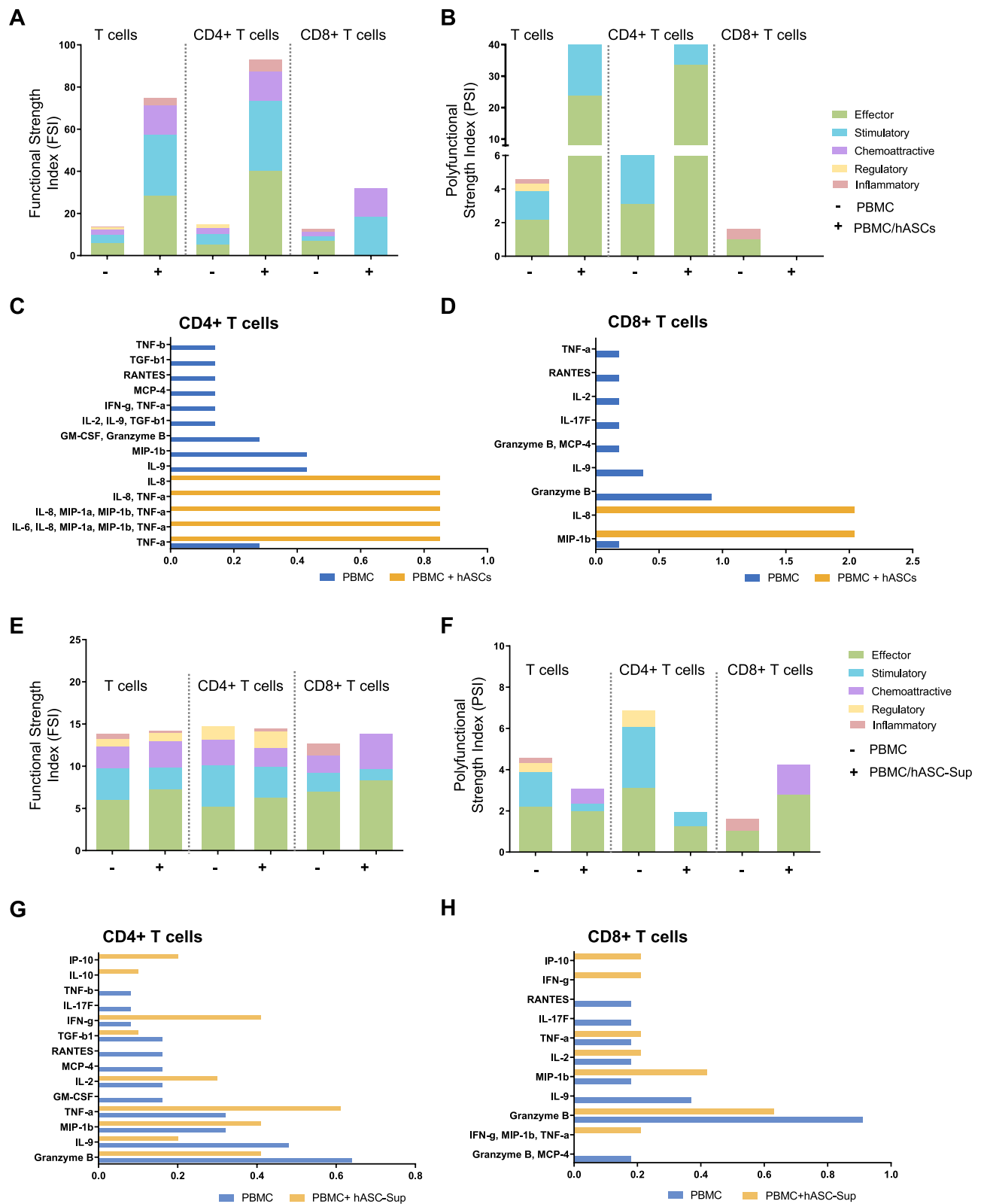
Fig. 6 (See legend on previous page.)

To evaluate the effect of hASC supernatants on T-cell functionality, activated PBMCs were cultured with or without hASC supernatants in vitro for 4 h, after which the FSI value, PSI value and cytokines secreted by CD4$^+$ T cells and CD8$^+$ T cells were determined. The results revealed that the functional profiles of CD4$^+$ T cells and CD8$^+$ T cells also changed when the cells were cultured with supernatants from hASCs (Fig. 6E). The effector, stimulatory and regulatory function PSI values of CD4$^+$ T cells decreased when the cells were cultured with the medium from hASCs (Fig. 6F). The cytokines and chemokines produced by CD4$^+$ T cells whose levels were most strongly decreased were Granzyme B, IL-9, TGF-β1, IL-17F, and TNF-β after culture with medium from hASCs (Fig. 6G). The effector PSI and chemoattractive PSI values of CD8$^+$ T cells were increased, but the inflammatory PSI value was increased when these cells were cultured with medium from hASCs (Fig. 6F). Polyfunctionality analysis revealed that the number of CD8$^+$ T cells that secreted multiple factors (IFN-γ, MIP-1beta and TNF-α) was increased, whereas the number of cells that secreted both Granzyme B and MCP-4 was decreased after culture with supernatants from hASCs (Fig. 6H). Single-cell PAT principal component analysis (PCA) revealed the polyfunctionality landscape of T cells, as presented in Fig. S8.

To further assess the impact of DPP4 expression in hASCs on the regulation of T-cell functionality, activated PBMCs were cultured with or without DPP4$^-$ hASCs and DPP4$^+$ hASCs supernatants or cells. The results revealed that CD8$^+$ T cell PSI values, including effector, stimulatory, chemoattractive and inflammatory values, were significantly greater in the DPP4$^+$ hASC-treated group than in the DPP4$^-$ hASC-treated group (Fig. 7A, B). Compared with those observed after treatment with DPP4$^-$ hASCs, the number of CD4$^+$ T cells that secreted single cytokines, including MIP-1beta, IL-8 and TNF-α, was greater after treatment with the DPP4$^+$ hASCs (Fig. 7C). Compared with DPP4$^-$ hASCs, DPP4$^+$ hASCs promoted the secretion of multiple factors, including IL-8, MIP-1alpha, MIP-1beta, and TNF-α; Granzyme B and MIP-1beta; IL-6 and IL-8, and secretion of single cytokines,

including MIP-1beta and Granzyme B, by CD8$^+$ T cell (Fig. 7D). These findings indicated that the regulation of CD8$^+$ T-cell functionality by DPP4$^+$ hASCs was stronger than that by DPP4$^-$ hASCs.

An analysis of the effects of supernatants derived from DPP4$^-$ hASCs and DPP4$^+$ hASCs on the functional properties of T cells revealed that the FSI and PSI values of CD4$^+$ T cells and CD8$^+$ T cells were greater in those cultured with supernatants of DPP4$^+$ hASCs than in those cultured with the supernatants of DPP4$^-$ hASCs (Fig. 7E, F). Compared with those of cells cultured with the supernatant of DPP4$^-$ hASCs, the effector PSI values of CD4$^+$ T cells and the effector PSI values and stimulatory PSI values of CD8$^+$ T cells were greater when the cells were cultured with the supernatant of DPP4$^+$ hASCs (Fig. 7F). Compared with those in cultures with the supernatant of DPP4$^-$ hASCs, the regulatory and inflammatory functionas of CD8$^+$ T cells were lower in cultures with the supernatant of DPP4$^+$ hASCs (Fig. 7F).

Compared with those cultured with supernatants derived from DPP4$^-$ hASCs, the percentages of CD4$^+$ T cells that secreted MIP-1beta and TNF-α were higher, whereas the percentages of cells that secreted Granzyme B and perforin were lower upon treatment with supernatants derived from DPP4$^+$ hASCs (Fig. 7G). The number of CD8$^+$ T cells that secreted TNF-α, IL-8, and MIP-1alpha was greater, the number of cells that secreted Granzyme B and MIP-1beta, and the number of cells that secreted IL-17A, TNF-α, and TNF-β was lower among cells cultured with supernatants derived from DPP4$^+$ hASCs than among those cultured with supernatants derived from DPP4$^-$ hASCs (Fig. 7H).

To further assess the impact of DPP4 expression in hASCs on the regulation of T-cell functionality, activated PBMCs were cultured with control siRNA-treated DPP4$^+$ hASCs and DPP4 siRNA-treated DPP4$^+$ hASCs. The results revealed that the effector, inflammatory and stimulatory functions were decreased in both CD4$^+$ T cells and CD8$^+$ T cells upon treatment with DPP4 siRNA-treated DPP4$^+$ hASCs compared with those in control siRNA-treated DPP4$^+$ hASCs (Fig. 8A, B). Compared with that of control siRNA-treated DPP4$^+$ hASCs,

(See figure on next page.)

Fig. 7 Regulation of the polyfunctionality of T cells by DPP4$^-$ hASCs and DPP4$^+$ hASCs. **A** Stacked bar charts showing the single-cell functionality of PBMCs cocultured with DPP4$^-$ hASCs and DPP4$^+$ hASCs. **B** Stacked bar charts showing the single-cell polyfunctionality of PBMCs cocultured with DPP4$^-$ hASCs and DPP4$^+$ hASCs; each colour corresponds to a specific cytokine or combination of cytokines. **C** Histogram showing the polyfunctional group of CD4$^+$ T cells cocultured with DPP4$^-$ hASCs and DPP4$^+$ hASCs. **D** Histogram showing the polyfunctional group of CD8$^+$ T cells cocultured with DPP4$^-$ hASCs and DPP4$^+$ hASCs. **E** Stacked bar charts showing the single-cell functionality of PBMCs treated with the supernatant of DPP4$^-$ hASCs and DPP4$^+$ hASCs. **F** Stacked bar charts showing the single-cell polyfunctionality of PBMCs treated with the supernatant of DPP4$^-$ hASCs and DPP4$^+$ hASCs; each colour corresponds to a specific cytokine or combination of cytokines. **G** Histogram showing the polyfunctional group of CD4$^+$ T cells treated with the supernatant of DPP4$^-$ hASCs and DPP4$^+$ hASCs. **H** Histogram showing the polyfunctional group of CD8$^+$ T cells treated with the supernatant of DPP4$^-$ hASCs and DPP4$^+$ hASCs
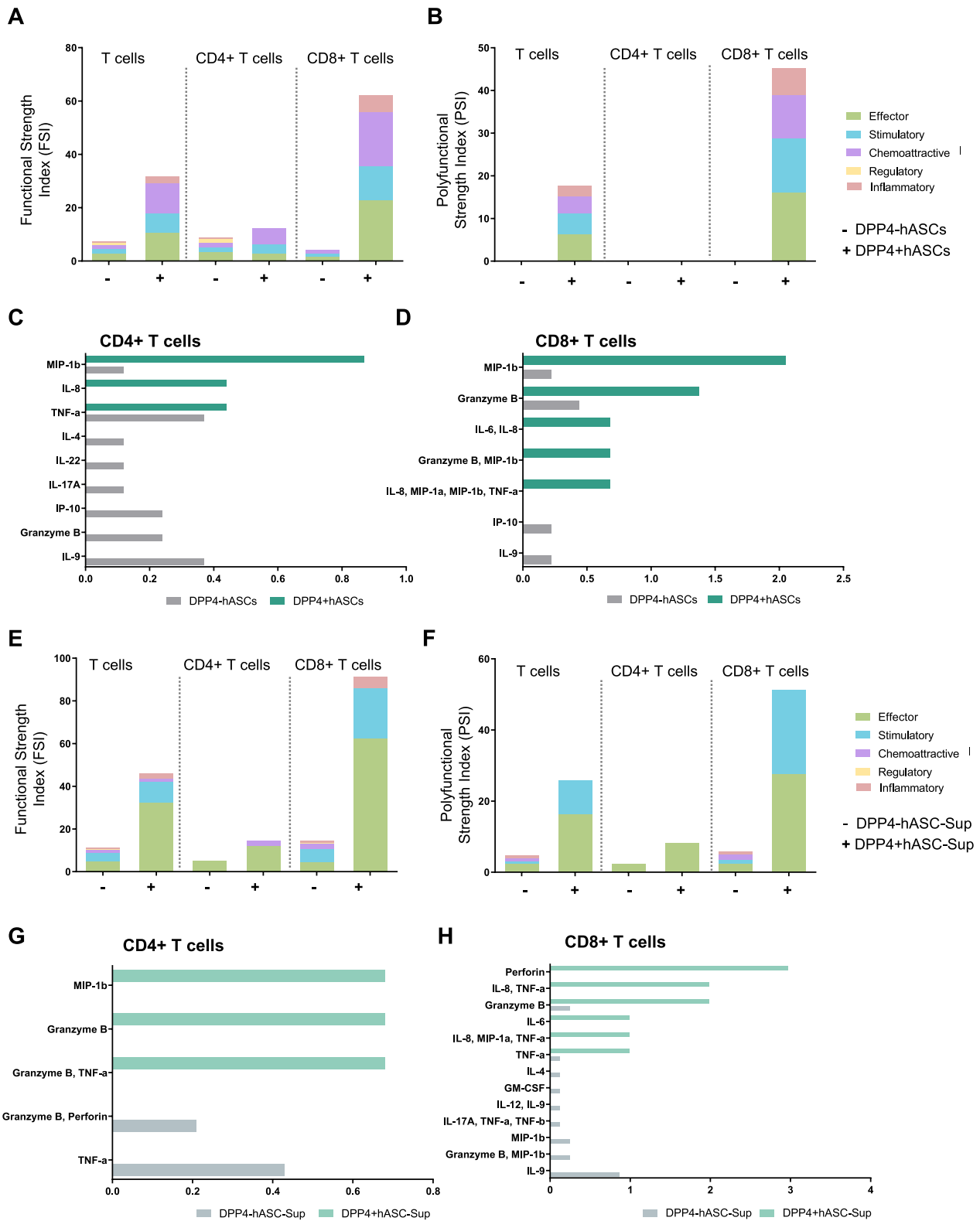
Fig. 7 (See legend on previous page.)

Zhang *et al. Stem Cell Research & Therapy*   (2024) 15:338

Page 16 of 20

the polyfunctionality of CD4$^+$ T cells was decreased upon treatment with DPP4 siRNA-treated DPP4$^+$ hASCs (Fig. 8B). The regulatory PSI value of CD8$^+$ T cells was greater in DPP4 siRNA-treated DPP4$^+$ hASCs than in control siRNA-treated DPP4$^+$ hASCs (Fig. 8B). The analysis of polyfunctionality revealed that most of CD4$^+$ T cells and CD8$^+$ T cells secreted factors such as GM-CSF, Granzyme B, IL-8, MIP-1alpha, MIP-1beta and TNF-α; however, the IL-6, IL-8, MIP-1alpha, MIP-1beta, and TNF-α levels were lower after culture with DPP4 siRNA-treated DPP4$^+$ hASCs than after culture with control siRNA-treated DPP4$^+$ hASCs (Fig. 8C, D). The secretion of factors, such as IL-22, IP-10, IL-4 and IL-9 by CD8$^+$ T cells was increased upon treatment with DPP4 siRNA-treated DPP4$^+$ hASCs (Fig. 8D). These data were similar to those of the cells cultured with DPP4$^-$ hASCs and DPP4$^+$ hASCs (Fig. 7C, D).

Analysis of the polyfunctionality of T cells cultured with medium derived from control siRNA-treated DPP4$^+$ hASCs and DPP4 siRNA-treated DPP4$^+$ hASCs revealed that the numbers of inflammatory, chemoattractive, stimulatory, and effector CD8$^+$ T cells were decreased (Fig. 8E, F). Compared with those of cells cultured with supernatants derived from control siRNA-treated hASCs, the percentages of CD4$^+$ T cells that secreted cytokines such as GM-CSF, Granzyme B, IL-8, MIP-1alpha, MIP-1beta and TNF-α or IL-6, IL-8, alpha, MIP-1beta, and TNF-α were lower, whereas the percentages of cells that secreted factors such as IL-6, IL-8, IP-10, MIP-1alpha, MIP-1beta, TNF-α, and TNF-β were greater among cells treated with supernatants derived from DPP4 siRNA-treated hASCs (Fig. 8G). The percentages of CD8$^+$ T cells that secreted polyfunctional factors, such as IL-6, MIP-1alpha, MIP-1beta, and TNF-α, IL-8, perforin, and TNF-α, decreased upon treatment with supernatants derived from DPP4 siRNA-treated hASCs (Fig. 8H).

These data confirmed that hASCs have stronger immunomodulatory effects on T-cell polyfunctionality than do their secreted factors. DPP4 expression in hASCs is involved in the regulation of CD4$^+$ T-cell and CD8$^+$ T-cell polyfunctionality. CD8$^+$ T cells are more sensitive to the cellular regulation of hASCs, especially the expression of DPP4 in hASCs.

Discussion

Evidence has shown that hASCs are an ideal autologous adult stem cell source that provides unprecedented opportunities for the development of cell therapies for intractable diseases and injuries. Therefore, practical issues that limit their use, including their inherent heterogeneity, should be carefully considered [4, 41, 42].

The heterogeneity of hASCs is related to many factors, including the sex, the health status of the donors, and the different adipose depots from which they are isolated, such as subcutaneous and visceral WAT [9, 10, 30]. Moreover, recent work has shown that hASCs isolated from a single WAT depot are not a homogeneous population [42]. Given that the heterogeneous properties of these cells are closely related to their suitability for therapeutics, clearly defining the cell type being utilized will become increasingly important in clinical applications [4].

Single-cell RNA sequencing and cell trajectory analyses revealed that the DPP4$^+$ and ICAM1$^+$ hASC populations presented distinct proliferative and adipogenic differentiation properties [15]. In the present study, we demonstrated that DPP4$^+$ and DPP4$^-$ hASCs derived from subcutaneous WAT exhibit distinct proliferative and hepatic differentiation abilities, inflammatory factor secretion profiles and immunomodulatory functions. DPP4$^+$ hASCs have a lower proliferative ability, with higher expression of cellular senescence markers. Knockdown of DPP4 in DPP4$^+$ hASCs increased their proliferation ability and decreased the proportion of senescent cells. Similarly, DPP4 is more highly expressed in senescent cells [14, 16].

Previously, we demonstrated that hASCs have the potential to differentiate into functional hepatocytes [19, 39]. Here, we confirmed that the differentiation efficiency

(See figure on next page.)

Fig. 8 Regulation of the polyfunctionality of T cells by DPP4$^+$ hASCs treated with DPP4 siRNA. **A** Stacked bar charts showing the single-cell functionality of PBMCs cocultured with DPP4$^+$ hASCs treated with control siRNA or DPP4 siRNA. **B** Stacked bar charts showing the single-cell polyfunctionality of PBMCs cocultured with DPP4$^+$ hASCs treated with control siRNA or DPP4 siRNA; each colour corresponds to a specific cytokine or combination of cytokines. **C** Histogram showing the polyfunctional group of CD4$^+$ T cells cocultured with DPP4$^+$ hASCs treated with control siRNA or DPP4 siRNA. **D** Histogram showing the polyfunctional group of CD8$^+$ T cells cocultured with DPP4$^+$ hASCs treated with control siRNA or DPP4 siRNA. **E** Stacked bar charts showing the single-cell functionality of PBMCs treated with the supernatants of DPP4$^+$ hASCs treated with control siRNA or DPP4 siRNA. **F** Stacked bar charts showing the single-cell polyfunctionality of PBMCs treated with the supernatant of DPP4$^+$ hASCs treated with control siRNA and DPP4 siRNA; each colour corresponds to a specific cytokine or combination of cytokines. **G** Histogram showing the polyfunctional group of CD4$^+$ T cells treated with the supernatants of DPP4$^+$ hASCs treated with control siRNA or DPP4 siRNA. **H** Histogram showing the polyfunctional group of CD8$^+$ T cells treated with the supernatant of DPP4$^+$ hASCs treated with control siRNA or DPP4 siRNA
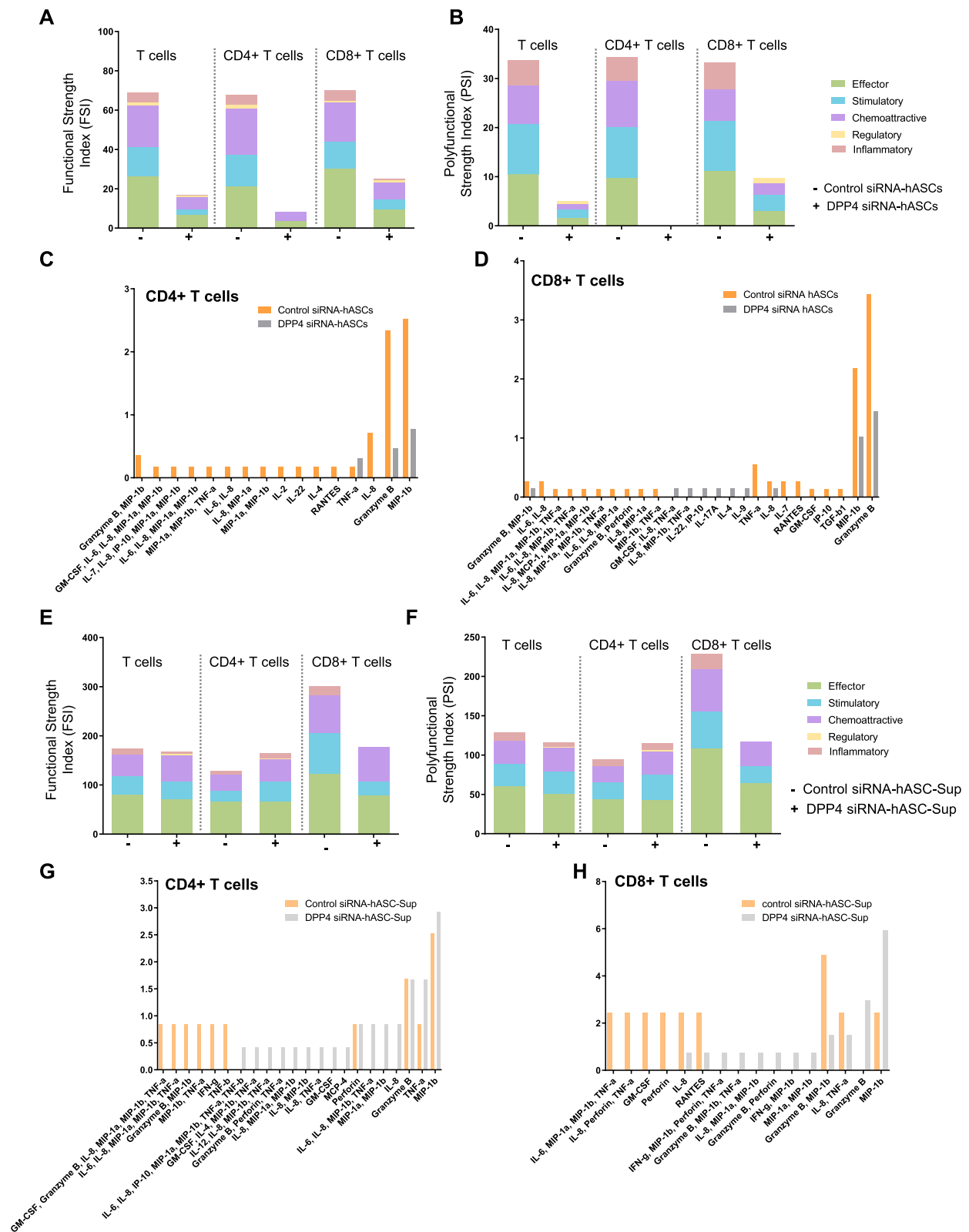
Fig. 8 (See legend on previous page.)

Zhang *et al. Stem Cell Research & Therapy*   (2024) 15:338

Page 18 of 20

of DPP4$^+$ hASCs increased at different stages, including the EPC, HPC and HLC stages. Considering that DPP4$^-$ hASCs may secrete more HGF than DPP4$^+$ hASCs do, we suggest that the expression of DPP4 in hASCs can regulate their differentiation capacity in an autocrine manner.

The increased levels of growth factors, cytokines, chemokines and soluble receptors secreted by DPP4$^+$ hASCs indicated that they may be involved in immunoregulatory and inflammatory processes. MIG is thought to mediate T-cell recruitment to valvular tissue lesions [43]. The chemotactic cytokine fractalkine (FKN, chemokine CX3CL1) has unique properties and strongly attracts T cells and monocytes. FKN signalling via CX3CR1 plays an important role in many processes related to inflammation and the immune response or occurs simultaneously and overlaps [44]. MIP-1 beta is most effective at augmenting the adhesion of CD8$^+$ T cells to the vascular cell adhesion molecule VCAM-1 [45]. GRO-alpha (CXCL1) is one of the most important chemokines involved in the development of many inflammatory diseases, such as the recruitment of neutrophils [46, 47]. Therefore, we speculate that DPP4$^+$ hASCs may play an important role in the regulation of T-cell functions. Notably, the expression of some cytokines, such as MMP-1, GRO-alpha, IL-6, and IL-8, in DPP4$^+$ hASCs did not decrease when DPP4 was knocked down by siRNA. We speculate that the expression of these cytokines in hASCs is indirectly regulated by DPP4 or by other compensatory mechanisms.

Our results indicated that the percentage of T-cell polyfunctionality significantly increased when T cells were cultured with the factors secreted by DPP4$^+$ hASCs. The percentage of CD8$^+$ T cells that secreted single cytokines, including perforin, Granzyme B, TNF-α, and IL-6, or secreted multiple factors, including IL-8 and TNF-α, IL-8, MIP-1alpha and TNF-α, was increased upon treatment with supernatants derived from DPP4$^+$ hASCs. However, the percentage of CD8$^+$ T cells that secreted single cytokines, including IL-9, MIP-1beta, GM-CSF, and IL-4, or secreted multiple factors, including MIP-1beta and Granzyme B; IL-17A, TNF-α and TNF-β; and IL-12 and IL-9, was lower upon treatment with supernatants derived from DPP4$^+$ hASCs than in the control group. These findings confirmed that DPP4$^+$ hASCs more intensely regulate the immune response of CD8$^+$ T cells.

Conclusion

DPP4 may regulate the proliferation, hepatocyte differentiation, inflammatory cytokine secretion and T-cell functionality of hASCs. These data provide a key foundation for understanding the important role of hASC subpopulation in the regulation of T cells, which may be helpful for future immune activation studies and allow them to be customized for clinical application.

Abbreviations

hASCs	Human adipose-derived stromal/stem cells
DPP4	Dipeptidyl peptidase-4
FACS	Fluorescence-activated cell sorting
VEGF-A	Vascular endothelial growth factor-A
MCP-1	Monocyte chemoattractant protein-1
IL-6	Interleukin 6
MMP	Matrix metalloproteinase
FKN	Fractalkine
GRO-alpha	Growth-related oncogene-alpha
MIG	Monokine induced by interferon-gamma
MIP	Macrophage inflammatory protein
M-CSF	Macrophage colony-stimulating factor
TNF-α	Tumour necrosis factor alpha
SVF	Stromal vascular fraction
HLCs	Hepatocyte-like cells
TGF-β1	Transforming growth factor-β1
HGF	Hepatocyte growth factor
SA-β-Gal	Senescence β-galactosidase
FSI	Functionality strength index
PSI	Polyfunctionality strength index
GLB1	The galactosidase beta 1
CDKN	Cyclin dependent kinase inhibitor
TP53	Tumor protein p53
IL1R1	Interleukin 1 receptor type 1
IGFBP3	Insulin like growth factor binding protein 3
EPCs	Definitive endodermal progenitor cells
HPCs	Hepatic progenitor cells
AFP	α-Fetoprotein
ALB	Albumin
GSTA2	Glutathione S-transferase alpha 2

Supplementary Information

The online version contains supplementary material available at https://doi.org/10.1186/s13287-024-03950-7.

Supplementary Material 1.

Supplementary Material 2.

Supplementary Material 3.

Supplementary Material 4.

Supplementary Material 5.

Supplementary Material 6.

Supplementary Material 7.

Author contributions

YZ was responsible for conception and design, collection and assembly of data, and data analysis. MH was responsible for conception and design, and collection and assembly of data. XM was responsible for data analysis. WL was responsible for administrative support. YC was responsible for data analysis. XH was responsible for collection and assembly of data. XH was responsible for collect adipose tissues of patients. HZ was responsible for conception

Zhang *et al. Stem Cell Research & Therapy*   (2024) 15:338

Page 19 of 20

Declarations

Ethics approval and consent to participate
All human WAT samples were obtained with informed patient consent and under the approval of IRB of Beijing Tiantan Hospital, Capital Medical University, China (Title of an ethical approved project, "Establishment of metabolic surgery clinical data and biological sample database", Approval number, KY2018-036-02 and date of approval, July 4, 2018). All experimental protocols were approved and carried out in accordance with the relevant guidelines and regulations of the Ethics Committee of Capital Medical University, China (Title of an ethical approved project, "Integrin signaling is involved in the adaptive regulatory mechanism of mitochondrial energy metabolism of adipose stem cells and hepatocytes in the process of persistent glucose and fatty acid metabolism remodelling", Approval number, 2019SY068, and date of approval, April 29, 2019). All investigations were conducted according to the principles expressed in the Declaration of Helsinki.

Consent for publication
All authors confirm their consent for publication.

Competing interests
The authors declare no competing interests.

Author details
[1]Department of Cell Biology, School of Basic Medical Science, Capital Medical University, Beijing 100069, China. [2]Biomedical Innovation Center, Beijing Shijitan Hospital, Capital Medical University, Beijing 100038, China. [3]Beijing Key Laboratory for Therapeutic Cancer Vaccines, Beijing Shijitan Hospital, Capital Medical University, Beijing 100038, China. [4]Experimental Center for Basic Medical Teaching, School of Basic Medical Science, Capital Medical University, Beijing 100069, China. [5]Fu Xing Hospital, Capital Medical University, Beijing 100038, China. [6]Department of Cell Biology, Capital Medical University, Beijing 100069, China.

References
1. Sakers A, De Siqueira MK, Seale P, Villanueva CJ. Adipose-tissue plasticity in health and disease. Cell. 2022;185(3):419–46.
2. Ceccarelli S, Pontecorvi P, Anastasiadou E, Napoli C, Marchese C. Immunomodulatory effect of adipose-derived stem cells: the cutting edge of clinical application. Front Cell Dev Biol. 2020;8:236.
3. Song N, Scholtemeijer M, Shah K. Mesenchymal stem cell immunomodulation: mechanisms and therapeutic potential. Trends Pharmacol Sci. 2020;41(9):653–64.
4. Sabol RA, Bowles AC, Cote A, Wise R, Pashos N, Bunnell BA. Therapeutic potential of adipose stem cells. Adv Exp Med Biol. 2021;1341:15–25.
5. Zhao Q, Han Z, Wang J. Development and investigational new drug application of mesenchymal stem/stromal cells products in China. Stem Cells Transl Med. 2021;10(Suppl 2):S18–30.
6. Hoang DM, Pham PT, Bach TQ, Ngo ATL, Nguyen QT, Phan TTK, et al. Stem cell-based therapy for human diseases. Signal Transduct Target Ther. 2022;7(1):1–41.
7. Han X, Ma Y, Lu X, Li W, Xia E, Li TC, et al. Transplantation of human adipose stem cells using acellular human amniotic membrane improves angiogenesis in injured endometrial tissue in a rat intrauterine adhesion model. Cell Transpl. 2020;29:963689720952055.
8. Yin JQ, Zhu J, Ankrum JA. Manufacturing of primed mesenchymal stromal cells for therapy. Nat Biomed Eng. 2019;3(2):90–104.
9. Ong WK, Chakraborty S, Sugii S. Adipose tissue: understanding the heterogeneity of stem cells for regenerative medicine. Biomolecules. 2021;11(7):918.
10. Maged G, Abdelsamed MA, Wang H, Lotfy A. The potency of mesenchymal stem/stromal cells: does donor sex matter? Stem Cell Res Ther. 2024;15(1):112.
11. Liu X, Xiang Q, Xu F, Huang J, Yu N, Zhang Q, et al. Single-cell RNA-seq of cultured human adipose-derived mesenchymal stem cells. Sci Data. 2019;6:190031.
12. Vijay J, Gauthier MF, Biswell RL, Louiselle DA, Johnston JJ, Cheung WA, et al. Single-cell analysis of human adipose tissue identifies depot and disease specific cell types. Nat Metab. 2020;2(1):97–109.
13. Torrecillas-Baena B, Galvez-Moreno MA, Quesada-Gomez JM, Dorado G, Casado-Diaz A. Influence of dipeptidyl peptidase-4 (DPP4) on mesenchymal stem-cell (MSC) biology: implications for regenerative medicine–review. Stem Cell Rev Rep. 2022;18(1):56–76.
14. Kim KM, Noh JH, Bodogai M, Martindale JL, Yang X, Indig FE, et al. Identification of senescent cell surface targetable protein DPP4. Genes Dev. 2017;31(15):1529–34.
15. Merrick D, Sakers A, Irgebay Z, Okada C, Calvert C, Morley MP, et al. Identification of a mesenchymal progenitor cell hierarchy in adipose tissue. Science. 2019;364(6438):2501.
16. Psaroudis RT, Singh U, Lora M, Jeon P, Boursiquot A, Stochaj U, et al. CD26 is a senescence marker associated with reduced immunopotency of human adipose tissue-derived multipotent mesenchymal stromal cells. Stem Cell Res Ther. 2022;13(1):358.
17. Rennert RC, Januszyk M, Sorkin M, Rodrigues M, Maan ZN, Duscher D, et al. Microfluidic single-cell transcriptional analysis rationally identifies novel surface marker profiles to enhance cell-based therapies. Nat Commun. 2016;7(1):11945.
18. Stefkovich M, Traynor S, Cheng L, Merrick D, Seale P. Dpp4$^+$ interstitial progenitor cells contribute to basal and high fat diet-induced adipogenesis. Mol Metab. 2021;54:101357.
19. Li X, Yuan J, Li W, Liu S, Hua M, Lu X, et al. Direct differentiation of homogeneous human adipose stem cells into functional hepatocytes by mimicking liver embryogenesis. J Cell Physiol. 2014;229(6):801–12.
20. Yuan J, Li W, Huang J, Guo X, Li X, Lu X, et al. Transplantation of human adipose stem cell-derived hepatocyte-like cells with restricted localization to liver using acellular amniotic membrane. Stem Cell Res Ther. 2015;6:217.
21. Guo X, Li W, Ma M, Lu X, Zhang H. Endothelial cell-derived matrix promotes the metabolic functional maturation of hepatocyte via integrin-Src signalling. J Cell Mol Med. 2017;21(11):2809–22.
22. Hu C, Zhao L, Li L. Current understanding of adipose-derived mesenchymal stem cell-based therapies in liver diseases. Stem Cell Res Ther. 2019;10(1):199.
23. Aurich H, Sgodda M, Kaltwasser P, Vetter M, Weise A, Liehr T, et al. Hepatocyte differentiation of mesenchymal stem cells from human adipose tissue in vitro promotes hepatic integration in vivo. Gut. 2009;58(4):570–81.
24. Jin Y, Zhang J, Xu Y, Yi K, Li F, Zhou H, et al. Stem cell-derived hepatocyte therapy using versatile biomimetic nanozyme incorporated nanofiber-reinforced decellularized extracellular matrix hydrogels for the treatment of acute liver failure. Bioact Mater. 2023;28:112–31.
25. Hwang Y, Goh M, Kim M, Tae G. Injectable and detachable heparin-based hydrogel micropatches for hepatic differentiation of hADSCs and their liver targeted delivery. Biomaterials. 2018;165:94–104.
26. Bi G, Zhang X, Li W, Lu X, He X, Li Y, et al. Modeling alcohol-associated liver disease in humans using adipose stromal or stem cell-derived organoids. Cell Rep Methods. 2024;4:100778.

Zhang *et al. Stem Cell Research & Therapy*   (2024) 15:338

Page 20 of 20

27. Li Y, Lin Y, Han X, Li W, Yan W, Ma Y, et al. GSK3 inhibitor ameliorates steatosis through the modulation of mitochondrial dysfunction in hepatocytes of obese patients. iScience. 2021;24(3):102149.
28. Cawthorn WP, Scheller EL, MacDougald OA. Adipose tissue stem cells: the great WAT hope. Trends Endocrinol Metab. 2012;23(6):270–7.
29. Serena C, Keiran N, Ceperuelo-Mallafre V, Ejarque M, Fradera R, Roche K, et al. Obesity and type 2 diabetes alters the immune properties of human adipose derived stem cells. Stem Cells. 2016;34(10):2559–73.
30. Han X, Li W, He X, Lu X, Zhang Y, Li Y, et al. Blockade of TGF-β signalling alleviates human adipose stem cell senescence induced by native ECM in obesity visceral white adipose tissue. Stem Cell Res Ther. 2023;14(1):291.
31. Franquesa M, Mensah FK, Huizinga R, Strini T, Boon L, Lombardo E, et al. Human adipose tissue-derived mesenchymal stem cells abrogate plasmablast formation and induce regulatory B cells independently of T helper cells. Stem Cells. 2015;33(3):880–91.
32. Zhou K, Guo S, Tong S, Sun Q, Li F, Zhang X, et al. Immunosuppression of human adipose-derived stem cells on T cell subsets via the reduction of NF-kappaB activation mediated by PD-L1/PD-1 and Gal-9/TIM-3 pathways. Stem Cells Dev. 2018;27(17):1191–202.
33. Wu F, Wu F, Zhou Q, Liu X, Fei J, Zhang D, et al. A CCL2+ DPP4+ subset of mesenchymal stem cells expedites aberrant formation of creeping fat in humans. Nat Commun. 2023;14(1):5830.
34. Ma Y, Ma M, Sun J, Li W, Li Y, Guo X, et al. CHIR-99021 regulates mitochondrial remodelling via beta-catenin signalling and miRNA expression during endodermal differentiation. J Cell Sci. 2019;132(15):229948.
35. Xu D, Jiang Y, Lun W, Cao Y, Xu X, Wang B, et al. Characteristic profiling of soluble factors in the cerebrospinal fluid of patients with neurosyphilis. J Infect Dis. 2024;230:221–30.
36. Lawlor N, Nehar-Belaid D, Grassmann JDS, Stoeckius M, Smibert P, Stitzel ML, et al. Single cell analysis of blood mononuclear cells stimulated through either LPS or anti-CD3 and anti-CD28. Front Immunol. 2021;12:636720.
37. Parisi G, Saco JD, Salazar FB, Tsoi J, Krystofinski P, Puig-Saus C, et al. Persistence of adoptively transferred T cells with a kinetically engineered IL-2 receptor agonist. Nat Commun. 2020;11(1):660.
38. Rossi J, Paczkowski P, Shen Y-W, Morse K, Flynn B, Kaiser A, et al. Preinfusion polyfunctional anti-CD19 chimeric antigen receptor T cells are associated with clinical outcomes in NHL. Blood. 2018;132(8):804–14.
39. Huang J, Guo X, Li W, Zhang H. Activation of Wnt/beta-catenin signalling via GSK3 inhibitors direct differentiation of human adipose stem cells into functional hepatocytes. Sci Rep. 2017;7:40716.
40. Seder RA, Darrah PA, Roederer M. T-cell quality in memory and protection: implications for vaccine design. Nat Rev Immunol. 2008;8(4):247–58.
41. Yamanaka S. Pluripotent stem cell-based cell therapy-promise and challenges. Cell Stem Cell. 2020;27(4):523–31.
42. Cleal L, Aldea T, Chau YY. Fifty shades of white: understanding heterogeneity in white adipose stem cells. Adipocyte. 2017;6(3):205–16.
43. Faé KC, Palacios SA, Nogueira LG, Oshiro SE, Demarchi LMF, Bilate AMB, et al. CXCL9/Mig mediates T cells recruitment to valvular tissue lesions of chronic rheumatic heart disease patients. Inflammation. 2013;36(4):800–11.
44. Szukiewicz D. CX3CL1 (Fractalkine)-CX3CR1 axis in inflammation-induced angiogenesis and tumorigenesis. Int J Mol Sci. 2024;25(9):4679.
45. Tanaka Y, Adams DH, Hubscher S, Hirano H, Siebenlist U, Shaw S. T-cell adhesion induced by proteoglycan-immobilized cytokine MIP-lβ. Nature. 1993;361(6407):79–82.
46. Michael BD, Bricio-Moreno L, Sorensen EW, Miyabe Y, Lian J, Solomon T, et al. Astrocyte- and neuron-derived CXCL1 drives neutrophil transmigration and blood-brain barrier permeability in viral encephalitis. Cell Rep. 2020;32(11):108150.
47. Korbecki J, Barczak K, Gutowska I, Chlubek D, Baranowska-Bosiacka I. CXCL1: gene, promoter, regulation of expression, mRNA stability, regulation of activity in the intercellular space. Int J Mol Sci. 2022;23(2):792.

Publisher's Note